

Best theory diagram for metallic and laminated composite plates

Original

Best theory diagram for metallic and laminated composite plates / Petrolo, Marco; Lamberti, Alessandro; Miglioretti, Federico. - In: MECHANICS OF ADVANCED MATERIALS AND STRUCTURES. - ISSN 1537-6494. - STAMPA. - 23:9(2016), pp. 1114-1130. [10.1080/15376494.2015.1121525]

Availability:

This version is available at: 11583/2637607 since: 2020-04-24T13:47:30Z

Publisher:

J. N. Reddy

Published

DOI:10.1080/15376494.2015.1121525

Terms of use:

This article is made available under terms and conditions as specified in the corresponding bibliographic description in the repository

Publisher copyright

Taylor and Francis postprint/Author's Accepted Manuscript

This is an Accepted Manuscript of an article published by Taylor & Francis in MECHANICS OF ADVANCED MATERIALS AND STRUCTURES on 2016, available at <http://www.tandfonline.com/10.1080/15376494.2015.1121525>

(Article begins on next page)

Best Theory Diagram for Metallic and Laminated Composite Plates

M. Petrolo^{a*} A. Lamberti^{b†} F. Miglioretti^{b‡}

^aSchool of Aerospace, Mechanical and Manufacturing Engineering, RMIT University,
PO Box 71, Bundoora VIC 3083, Australia

^bDepartment of Mechanical and Aerospace Engineering, Politecnico di Torino,
Corso Duca degli Abruzzi 24, 10129 Torino, Italy.

Accepted Paper:

Special Issue of Mechanics of Advanced Materials and Structures
"Applications of Unified Formulation and Advanced Theories by
Various Numerical Approaches"

Author for correspondence:

M. Petrolo, Phd, Research Fellow,
School of Aerospace, Mechanical and Manufacturing Engineering,
RMIT University,
PO Box 71,
Bundoora VIC 3083, Australia,
tel: +61 3 992 56630,
e-mail: marco.petrolo@rmit.edu.au,
website: www.mul2.com

*Research Fellow, e-mail: marco.petrolo@rmit.edu.au

†PhD Student, e-mail: alessandro.lamberti@polito.it

‡Research Assistant, e-mail: federico.miglioretti@polito.it

Abstract

Best Theory Diagrams (BTDs) are reported in this paper for the static analysis of metallic and laminated composite plates. A BTD is a curve that synthetically provides the minimum number of unknown variables of a structural theory for a fixed error. The error is related to a given variable with respect to an exact or quasi-exact solution. The theories that belong to the BTD have been obtained by means of the Axiomatic/Asymptotic technique, and a genetic algorithm has been employed to obtain the BTD. The Carrera Unified Formulation (CUF) has been employed to obtain refined models, since the CUF can generate automatically, and in a unified manner, any type of plate model. Equivalent Single Layer (ESL) and Layer Wise (LW) kinematics are discussed. Closed-form, Navier - type solutions have been employed, and attention has therefore been restricted to simply-supported plates. The influence of various geometries, material properties and layouts has been considered, and their influence on the BTD has been evaluated. Furthermore, some known theories have been evaluated and compared with the BTD curve. The results suggest that the BTD and the CUF can be considered as tools to evaluate the accuracy of any structural theory against a reference solution in a systematic manner.

1 Introduction

Laminated composite and metallic plates are widely employed in several engineering applications. An accurate analysis of such structures is fundamental for a realistic and reliable structural design. Several mathematical tools are currently available. The solution of 3D elasticity equations offers the most accurate evaluation of the elastic response, but the computational cost can be significantly high. As an alternative, a 2D approach can be used. In the field of 2D approaches for plate analysis, the first model that was developed was the Kirchhoff-Love model ([1], [2]). According to this model, the thickness strain and the transverse shear deformations are neglected. The Classical Lamination Theory (CLT) belongs to this group. Improved theories can be obtained if at least one of Kirchhoff's hypotheses is removed. For example, a constant through-the-thickness transverse shear deformation can be taken into consideration. This is the case of the Reissner-Mindlin theories ([3], [4]), also known as the First-Order Shear Deformation Theory (FSDT). Further improvements have been introduced in Vlasov's ([5]) or Hildebrand-Reissner-Thomas's theories ([6]), which are based on higher-order expansions of the displacement components on the reference surface. The transverse stress and displacement components in a multilayer plate are continuous functions along the z direction; these significant particular features of layered structures were defined as C_z^0 -requirement in [7, 8]. The continuous displacement field is defined as the Zig-Zag effect (ZZ), and the transverse stress continuity at the interfaces is defined as Interlaminar-Continuity (IC). These two particular features make classical models inefficient for the analysis of multilayered plates, since they were originally developed for metallic one-layered plates. Moreover, classical models can be inaccurate for thick plate analysis.

Several refined models have been proposed in order to consider ZZ and IC effects. As reported in [9], the first scientist who proposed a theory that was able to provide the Zig-Zag condition was Lekhnitskii ([10]) who, in 1935, proposed a Zig-Zag solution for the analysis of multilayered beams. Another author who proposed a Zig-Zag theory was Ambartsumian ([11]). He extended the Reissner-Mindlin theory to layered, anisotropic plates and shells. Another author who made a fundamental contribution to the analysis of multilayered plates and shells is Reissner, who proposed a variational theorem that provides interlaminar continuity of transverse stresses ([12, 13, 14, 15]). It should be mentioned that a distinction among plate models should be made. As reported in the book by Reddy [16], it is possible to define the Equivalent Single Layer (ESL) and the Layer Wise (LW) approaches. According to the ESL approach, a plate/shell model can be analyzed considering it as a single equivalent lamina. In this case, the number of unknowns is independent of the number of layers of the plate/shell. In the LW approach, the displacement field is defined independently in each layer and the continuity at the interfaces is imposed. In this case, the number of unknowns depends on the number of layers of a plate/shell. The present work is embedded in the framework of the Carrera Unified Formulation (CUF). According to the CUF, the displacement field, in the case of plate analysis, is defined as an expansion of the thickness coordinate. The governing equations are defined in terms of a few fundamental nuclei whose form does not depend on the particular expansion order that is employed. Further details can be found in these books [17, 18, 19]. The CUF has been developed for plates and shells according to both ESL and LW approaches, as reported in [20], and both the Finite Element Method and closed-form Navier-type solutions have been employed. Examples can be found in [20]. The use of a refined theory for the analysis of plates leads to a better response analysis but, on the other hand, a higher computational cost is required. The possibility of obtaining accurate results for the analysis of plates/shells and, at the same time, of lowering the computational cost is offered by the axiomatic/asymptotic technique, developed by Carrera and Petrolo, and reported in [21]. The key idea of this technique is that, for a given problem, some terms of a refined model do not contribute to the evaluation of the behavior of a structure; in other words, if these terms are deactivated, it is possible to reduce the computational cost without degrading the accuracy of the full model. In [21], the technique was based on the deactivation of one displacement variable at a time, and the measurement of the introduced error was performed with respect to a reference solution. The effectiveness of a term was defined according to an a-priori error threshold: if the error was below that threshold, the term was considered not to be critical and was discarded. In that case, reduced

models were obtained for several kinds of plates (according to the material properties and the geometry). It was found that the material properties and the geometry influence the number and the order of the retained terms. Examples of axiomatic / asymptotic analyses can be found in [22], where the authors evaluated refined plate models, and the Finite Element Method was employed. Refined models for beams have also been considered, and the results are reported in [23] and in [24]. In particular in [24], the authors analyzed the influence of each displacement variable in the evaluation of the frequencies of beams. One of the latest works on axiomatic / asymptotic techniques is reported in [25], where the authors obtained LW reduced models and proposed some new criteria for the evaluation of the error. As in the previous works on reduced models for plates, the results showed that the number and the order of the retained terms were dependent to a great extent on the studied problem. Moreover, the authors analyzed refined models for multilayer shells in [26]; both ESL and LW models were analyzed, and the influence of Murakami's function was also considered (the use of Murakami's function in the CUF is reported in [20]). In [27], the authors proposed and analyzed several criteria for the measurement of the error.

In [28], the authors analyzed some refined models for isotropic plates by means of the axiomatic/asymptotic technique, and considered several boundary conditions and loading conditions. The authors analyzed the influence of the accuracy on the selection of terms by varying the error: as a result, several reduced models were obtained, and they were reported in an "Error vs Number of Degrees of Freedom" Cartesian plane (E/NDOFs plane). The result was a curve which has been defined as the Best Theory Diagram, which can be employed to determine the effectiveness of a given theory in terms of accuracy and computational cost. In one case, the errors of all the reduced models obtainable as a combination of the model terms were computed, and it was demonstrated that the BTD represents the best theory (in other words, the least cumbersome) for a given error. BTDs were systematically obtained and discussed in [29]: refined models for multilayered plates were considered, and the influence of several parameters (such as geometry and boundary conditions) was considered. It was demonstrated that the geometry, boundary conditions and material properties of a plate influence the BTDs. In that work, the Finite Element technique was employed and a genetic-like algorithm was used to obtain the BTDs.

In this work, BTDs are obtained for several types of plates. Unlike from the work reported in [28] and in [29], Navier-type, closed-form solutions are employed and LW models are analyzed. The use of the closed-form solution makes it possible to consider a large number of reduced models with a minimal computational effort: this fact is exploited in order to construct a number of BTDs. In addition, in some cases, the errors of all the obtainable reduced models are computed and presented in the Error/NDOFs plane: in this case, it is possible to assess the proposed BTDs and to analyze the error distribution. In addition, in some cases, some refined models that are available in the scientific literature are analyzed and positioned in the above mentioned Cartesian plane in order to highlight their accuracy.

The BTDs are obtained by means of a genetic algorithm. The use of such an algorithm was first proposed by Holland and his co-workers in the 1960s and 1970s ([30]). An overview of the multiple-objective optimization method, using genetic algorithms, is presented in [31] and in [32]. An overview of the use of genetic algorithms in engineering is presented in [33]. The paper is organized as follows: the considered theories are presented in Section 2 and the governing equations are introduced in Section 3. The axiomatic/asymptotic technique is introduced and the implementation of the genetic algorithm is discussed in Section 4. The results are commented in Section 5 and the conclusions are discussed in Section 6.

2 Carrera Unified Formulation for Plates

The plate geometry is reported in Fig. 1, the reference surface is denoted as Ω and its boundary as Γ . The reference system axes which belong to the reference surface Ω are denoted as x , y , and z is the reference axis normal to the reference surface. The length side dimensions of the plate are indicated as a and b and the thickness of the plate is defined as h .

In the framework of the Carrera Unified Formulation the displacement field of a plate can

be described as

$$\mathbf{u}(x, y, z) = F_\tau(z) \cdot \mathbf{u}_\tau(x, y) \quad \tau = 1, 2, \dots, M \quad (1)$$

where \mathbf{u} is the displacement vector ($u_x \ u_y \ u_z$) whose components are the displacements along the x, y, z reference axes. F_τ are the expansion functions and $\mathbf{u}_\tau = (u_{\tau x}, u_{\tau y}, u_{\tau z})$ are the displacement variables. M is the number of terms of the expansion. The expansion functions F_τ can be defined on the overall thickness of the plate or for each k -layer. In the former case Equivalent Single Layer (ESL) approach is followed and in the latter case a Layer Wise (LW) approach is used. Examples of ESL and LW schemes are reported in Figs. 2a and 2b respectively. A transverse section of a multilayered plate is reported, the number of layers is equal to N_L . A generic displacement component distribution is presented according to linear and higher-order expansions for these two approaches. In the following ESL and LW approaches are discussed in detail.

2.1 Equivalent Single Layer theory

According to the ESL scheme the behavior of a multilayered plate is analyzed considering it as a single equivalent lamina. In this case F_τ functions can be Mc-Laurin expansions of z defined as $F_\tau = z^{\tau-1}$. In the following the ESL models are synthetically indicated as EDN, where N is the expansion order. An example of an ED4 displacement field is reported

$$\begin{aligned} u_x &= u_{x1} + z u_{x2} + z^2 u_{x3} + z^3 u_{x4} + z^4 u_{x5} \\ u_y &= u_{y1} + z u_{y2} + z^2 u_{y3} + z^3 u_{y4} + z^4 u_{y5} \\ u_z &= u_{z1} + z u_{z2} + z^2 u_{z3} + z^3 u_{z4} + z^4 u_{z5} \end{aligned} \quad (2)$$

In the range of the ESL scheme, higher-order theories from open literature can be derived via CUF; some of these models are considered in this paper for comparison purposes. A first example can be the model proposed by Pandya (see [34]), the displacement components are:

$$\begin{aligned} u_x &= u_{x1} + z u_{x2} + z^2 u_{x3} + z^3 u_{x4} \\ u_y &= u_{y1} + z u_{y2} + z^2 u_{y3} + z^3 u_{y4} \\ u_z &= u_{z1} \end{aligned} \quad (3)$$

Another example is offered by Kant (see [35]), the displacement field is defined as:

$$\begin{aligned} u_x &= u_{x1} + z u_{x2} + z^2 u_{x3} + z^3 u_{x4} \\ u_y &= u_{y1} + z u_{y2} + z^2 u_{y3} + z^3 u_{y4} \\ u_z &= u_{z1} + z u_{z2} + z^2 u_{z3} + z^3 u_{z4} \end{aligned} \quad (4)$$

It is important to underline that CUF allows us to choose the higher-order terms to be included with no restrictions. For instance, one can consider a plate theory where incomplete fourth-order expansions are adopted:

$$\begin{aligned} u_x &= \quad + z u_{x2} + \quad + z^3 u_{x4} + z^4 u_{x5} \\ u_y &= \quad + z u_{y2} + z^2 u_{y3} + \quad + z^4 u_{y5} \\ u_z &= u_{z1} + z u_{z2} + z^2 u_{z3} + \quad + z^4 u_{z5} \end{aligned} \quad (5)$$

As mentioned in [21], classical models such as CLT and FSDT can be considered as special cases of the full linear expansion (ED1).

2.2 Layer Wise theory

According to the Layer Wise scheme the displacement field exhibits only C_0 -continuity through the laminate thickness. LW models can be conveniently built by using Legendre's polynomials expansion in each layer. The displacement field is described as

$$\mathbf{u}^k = F_t \cdot \mathbf{u}_t^k + F_b \cdot \mathbf{u}_b^k + F_r \cdot \mathbf{u}_r^k = F_\tau \mathbf{u}_\tau^k \quad \tau = t, b, r \quad r = 2, 3, \dots, N \quad k = 1, 2, \dots, N_l \quad (6)$$

where k is the generic k -layer of a plate and N_l is the number of the layers. Subscripts t and b correspond to the top and the bottom of a layer. Functions F_τ depend on a coordinate ζ_k , its range is $-1 \leq \zeta_k \leq 1$; its representation is reported in Fig. 2b. The extremal values -1 and 1 are reached at the bottom and at the top of the layer. Functions F_τ derive from the Legendre's polynomials according to the following equations.

$$F_t = \frac{P_0 + P_1}{2} \quad F_b = \frac{P_0 - P_1}{2} \quad F_r = P_r - P_{r-2} \quad r = 2, 3, \dots, N \quad (7)$$

The Legendre's polynomials for the fourth-order theory are

$$P_0 = 1 \quad P_1 = \zeta_k \quad P_2 = \frac{3\zeta_k^2 - 1}{2} \quad P_3 = \frac{5\zeta_k^3 - 3\zeta_k}{2} \quad P_4 = \frac{35\zeta_k^4}{8} - \frac{15\zeta_k^2}{4} + \frac{3}{8} \quad (8)$$

LW models ensure the compatibility of displacement at the interfaces 'zig-zag' effects by definition, that is

$$\mathbf{u}_t^k = \mathbf{u}_b^{k+1} \quad k = 1, \dots, N_l - 1 \quad (9)$$

In the following LW models are denoted by the acronym as LDN, where N is the expansion order. An example of LD4 layer displacement field is

$$\begin{aligned} u_x^k &= F_t u_{xt}^k + F_2 u_{x2}^k + F_3 u_{x3}^k + F_4 u_{x4}^k + F_b u_{xb}^k \\ u_y^k &= F_t u_{yt}^k + F_2 u_{y2}^k + F_3 u_{y3}^k + F_4 u_{y4}^k + F_b u_{yb}^k \\ u_z^k &= F_t u_{zt}^k + F_2 u_{z2}^k + F_3 u_{z3}^k + F_4 u_{z4}^k + F_b u_{zb}^k \end{aligned} \quad (10)$$

3 Governing equations and Navier-type solution

The analysis of a plate can be conducted by means of the Principle of Virtual Displacement (PVD) which states that:

$$\delta L_{int} = \delta L_{ext} \quad (11)$$

where δL_{int} is the virtual variation of the internal work, δL_{ext} is the virtual variation of the work made by the external loadings. Strain components can be grouped into in-plane (p) and out-of-plane (n) components, that is

$$\boldsymbol{\epsilon}_p^k = [\epsilon_{xx}^k \quad \epsilon_{yy}^k \quad \epsilon_{xy}^k]^T \quad \boldsymbol{\epsilon}_n^k = [\epsilon_{xz}^k \quad \epsilon_{yz}^k \quad \epsilon_{zz}^k]^T \quad (12)$$

where T denotes the transpose operation. This grouping leads to

$$\boldsymbol{\epsilon}_p^k = \mathbf{D}_p \mathbf{u}^k \quad \boldsymbol{\epsilon}_n^k = \mathbf{D}_n \mathbf{u}^k \quad (13)$$

by defining

$$\mathbf{D}_p = \begin{bmatrix} \frac{\partial}{\partial x} & 0 & 0 \\ 0 & \frac{\partial}{\partial y} & 0 \\ \frac{\partial}{\partial y} & \frac{\partial}{\partial x} & 0 \end{bmatrix} \quad (14)$$

$$\mathbf{D}_n = \begin{bmatrix} \frac{\partial}{\partial z} & 0 & \frac{\partial}{\partial x} \\ 0 & \frac{\partial}{\partial z} & \frac{\partial}{\partial y} \\ 0 & 0 & \frac{\partial}{\partial z} \end{bmatrix} = \overbrace{\begin{bmatrix} 0 & 0 & \frac{\partial}{\partial x} \\ 0 & 0 & \frac{\partial}{\partial y} \\ 0 & 0 & 0 \end{bmatrix}}^{\mathbf{D}_{n\Omega}} + \overbrace{\begin{bmatrix} \frac{\partial}{\partial z} & 0 & 0 \\ 0 & \frac{\partial}{\partial z} & 0 \\ 0 & 0 & \frac{\partial}{\partial z} \end{bmatrix}}^{\mathbf{D}_{nz}} \quad (15)$$

Stress components for a generic k layer can be obtained by means of the Hooke law,

$$\boldsymbol{\sigma}^k = \tilde{\mathbf{C}}^k \boldsymbol{\epsilon}^k \quad (16)$$

The dependence of the elastic coefficients \tilde{C}_{ij} on Young's modulus, Poisson's ratio, the shear modulus and the fiber angle is not reported. A detailed discussion is reported in the book by Reddy [16]. The stress components can be grouped into in-plane (p) and out-of-plane components as the strain components, i.e.

$$\boldsymbol{\sigma}_p^k = \begin{bmatrix} \sigma_{xx}^k & \sigma_{yy}^k & \sigma_{xy}^k \end{bmatrix}^T \quad \boldsymbol{\sigma}_n^k = \begin{bmatrix} \sigma_{xz}^k & \sigma_{yz}^k & \sigma_{zz}^k \end{bmatrix}^T \quad (17)$$

In this case the Hooke law can be defined as

$$\begin{aligned} \boldsymbol{\sigma}_p^k &= \tilde{\mathbf{C}}_{pp}^k \boldsymbol{\epsilon}_p^k + \tilde{\mathbf{C}}_{pn}^k \boldsymbol{\epsilon}_n^k \\ \boldsymbol{\sigma}_n^k &= \tilde{\mathbf{C}}_{np}^k \boldsymbol{\epsilon}_p^k + \tilde{\mathbf{C}}_{nn}^k \boldsymbol{\epsilon}_n^k \end{aligned} \quad (18)$$

In the case of orthotropic materials it is possible to write

$$\tilde{\mathbf{C}}_{pp}^k = \begin{bmatrix} \tilde{C}_{11}^k & \tilde{C}_{12}^k & \tilde{C}_{16}^k \\ \tilde{C}_{12}^k & \tilde{C}_{22}^k & \tilde{C}_{26}^k \\ \tilde{C}_{16}^k & \tilde{C}_{26}^k & \tilde{C}_{66}^k \end{bmatrix} \quad \tilde{\mathbf{C}}_{nn}^k = \begin{bmatrix} \tilde{C}_{55}^k & \tilde{C}_{45}^k & 0 \\ \tilde{C}_{45}^k & \tilde{C}_{44}^k & 0 \\ 0 & 0 & \tilde{C}_{33}^k \end{bmatrix} \quad \tilde{\mathbf{C}}_{pn}^k = \tilde{\mathbf{C}}_{np}^{kT} = \begin{bmatrix} 0 & 0 & \tilde{C}_{13}^k \\ 0 & 0 & \tilde{C}_{23}^k \\ 0 & 0 & \tilde{C}_{36}^k \end{bmatrix} \quad (19)$$

The virtual variation of the internal work can be computed as

$$\delta L_{int} = \delta L_{ext} \quad (20)$$

where δL_{int} is the virtual variation of the internal work and δL_{ext} is the virtual variation of the external work. The PVD can be written as

$$\sum_{k=1}^{N_l} \int_{\Omega_k} \int_{A_k} \left(\delta \boldsymbol{\epsilon}_p^{kT} \boldsymbol{\sigma}_p^k + \delta \boldsymbol{\epsilon}_n^{kT} \boldsymbol{\sigma}_n^k \right) dz d\Omega_k = \sum_{k=1}^{N_l} \delta L_{ext}^k \quad (21)$$

Further details about the CUF and its implementation through the use of variational principles can be found in [19].

The governing equations can be written as

$$\delta \mathbf{u}_s^k : \mathbf{K}_d^{k\tau s} \cdot \mathbf{u}_\tau^k = \mathbf{P}_\tau^k \quad (22)$$

and the boundary conditions are

$$\boldsymbol{\Pi}_d^{k\tau s} \mathbf{u}_\tau^k = \boldsymbol{\Pi}_d^{k\tau s} \bar{\mathbf{u}}_\tau^k \quad (23)$$

where \mathbf{P}_τ^k is the external load. The fundamental nucleus, $\mathbf{K}_d^{k\tau s}$ is assembled through the indexes τ and s . Superscript k denotes the assembly at the layer level. The explicit form of the fundamental nucleus is

$$\begin{aligned} \mathbf{K}_d^{k\tau s} = & \left\{ (-\mathbf{D}_p)^T \left[\tilde{\mathbf{C}}_{pp}^k E_{s\tau} \mathbf{D}_p + \tilde{\mathbf{C}}_{pn}^k E_{s\tau} \mathbf{D}_{n\Omega} + \tilde{\mathbf{C}}_{pn}^k E_{s\tau,z} \right] + \right. \\ & (-\mathbf{D}_{n\Omega})^T \left[\tilde{\mathbf{C}}_{pn}^{kT} E_{s\tau} \mathbf{D}_p + \tilde{\mathbf{C}}_{nn}^k E_{s\tau} \mathbf{D}_{n\Omega} + \tilde{\mathbf{C}}_{nn}^k E_{s\tau,z} \right] + \\ & \left. + \left[\tilde{\mathbf{C}}_{pn}^{kT} E_{s,z\tau} \mathbf{D}_p + \tilde{\mathbf{C}}_{nn}^k E_{s,z\tau} \mathbf{D}_{n\Omega} + \tilde{\mathbf{C}}_{nn}^k E_{s,z\tau,z} \right] \right\} \end{aligned} \quad (24)$$

and for the boundary conditions it is

$$\begin{aligned} \mathbf{\Pi}_d^{k\tau s} = & \left\{ (\mathbf{I}_p)^T \left[\mathbf{C}_{pp}^k E_{s\tau} \mathbf{D}_p + \mathbf{C}_{pp}^k E_{s\tau} \mathbf{A}_p + \mathbf{C}_{pn}^k E_{s\tau} \mathbf{D}_{n\Omega} + \mathbf{C}_{pn}^k E_{s\tau} \mathbf{A}_n + \mathbf{C}_{pn}^k E_{s\tau,z} \right] \right. \\ & \left. + (\mathbf{I}_{n\Omega})^T \left[\mathbf{C}_{pn}^{kT} E_{s\tau} \mathbf{D}_p + \mathbf{C}_{pn}^{kT} E_{s\tau} \mathbf{A}_p + \mathbf{C}_{nn}^k E_{s\tau} \mathbf{D}_{n\Omega} + \mathbf{C}_{nn}^k E_{s\tau} \mathbf{A}_n + \mathbf{C}_{nn}^k E_{s\tau,z} \right] \right\} H_\alpha^k H_\beta^k \end{aligned} \quad (25)$$

The analyses herein reported were based on the Navier closed-form solution for simply supported orthotropic plates, loaded by a transverse distribution of harmonic loadings. The following properties hold

$$\tilde{C}_{pp16} = \tilde{C}_{pp26} = \tilde{C}_{pn36} = \tilde{C}_{nn45} = 0 \quad (26)$$

The terms \mathbf{u}_τ^k for an LW model are expressed as:

$$\begin{aligned} u_{\alpha_\tau}^k &= \sum_{m,n} \hat{U}_{\alpha_\tau}^k \cdot \cos\left(\frac{m\pi\alpha_k}{a_k}\right) \sin\left(\frac{n\pi\beta_k}{b_k}\right) & k = 1, N_l \\ u_{\beta_\tau}^k &= \sum_{m,n} \hat{U}_{\beta_\tau}^k \cdot \sin\left(\frac{m\pi\alpha_k}{a_k}\right) \cos\left(\frac{n\pi\beta_k}{b_k}\right) & \tau = 1, M \\ u_{z_\tau}^k &= \sum_{m,n} \hat{U}_{z_\tau}^k \cdot \sin\left(\frac{m\pi\alpha_k}{a_k}\right) \sin\left(\frac{n\pi\beta_k}{b_k}\right) & m, n \in \mathbb{N} \end{aligned} \quad (27)$$

where $\hat{U}_{\alpha_\tau}^k$, $\hat{U}_{\beta_\tau}^k$ and $\hat{U}_{z_\tau}^k$ are the amplitudes, m and n are the numbers of waves (they range from 0 to ∞) and a_k and b_k are the plate lengths in the α_k and β_k directions, respectively. The same solution can be applied to the ESL approach, in this case the displacement variables appear without the superscript k .

4 The axiomatic/asymptotic method and the Best Theory Diagram

Accurate plate analyses can be obtained by increasing the order of the expansion. As a drawback, the computational cost could increase significantly with respect to the classical formulations. For a given problem, some terms of a refined model may not contribute to the evaluation of the behavior of a structure, as shown in [21]. In order to detect the ineffective variables for a given plate problem, the axiomatic/asymptotic method was introduced in that work. Through this method, it is possible to retrieve the ineffective terms in order to reduce the computational cost without accuracy penalties. In the following, the axiomatic/asymptotic technique is described, the Best Theory Diagram (BTD) is introduced and then a method to construct the BTD based on genetic algorithms is described.

4.1 Axiomatic/asymptotic technique

The possibility to construct reduced models is offered by the axiomatic/asymptotic technique which consists of the following steps:

1. parameters such as geometry, boundary conditions, loadings, materials and layer layouts are fixed;
2. a set of output parameters is chosen, such as displacement or stress components; in the following analyses σ_{xx} is considered;
3. a starting theory is fixed (axiomatic part), that is the displacement variables to be analyzed are defined; usually a theory which provides 3D-like solutions is chosen; a reference solution is defined (in the present work LD4 and ED4 approaches are adopted, since these fourth-order models offer an excellent agreement with the three-dimensional solutions as highlighted in [21] and in [25]);

4. the CUF is used to generate the governing equations for the considered theories;
5. the effectiveness of each term of the adopted expansion is evaluated by measuring the error due to its deactivation, a term is considered as ineffective if the error is negligible;
6. the most suitable structural model for a given structural problem is then obtained by discarding the non-effective displacement variables.

A graphical notation is introduced in order to synthetically represent the results. This consists of a table with three rows, and a number of columns equal to the number of the displacement variable used in the expansion. As an example, an LD4 model for a two layer shell is shown in Table 1 (full model). Table 1 also shows the reduced model in which the first layer term u_{z2}^1 and the second layer term u_{x2}^2 are deactivated. The meaning of the symbols are shown in Table 2. The symbol ■ is used to denote the terms that cannot be deactivated in the LW since this would introduce an extra constraint.

4.2 The Best Theory Diagram (BTD)

It is possible to associate to each reduced refined model the number of the active terms and its error computed with respect to a reference solution, as in Fig. 3. The error values are reported on the abscissa and the number of active terms is reported on the ordinate. Each black dot represents a reduced refined model and its position on the Cartesian plane is defined considering its error and the number of the active terms. In addition the synthetic representation of the active/non-active terms is reported for some reduced models. By considering all models, it is possible to note that some of them provide the lowest error for a given number of active terms. These models are labeled in Fig. 3 as 1, 2, 3, 4, 5 and they represent a Pareto front for the considered problems. This Pareto front is defined in this work as the Best Theory Diagram. The existence of such curve was already demonstrated in the work reported in [29]. This curve can be constructed for several problems, for example considering several type of materials, geometries and boundary conditions. BTD makes it possible to evaluate the minimum number of terms, N_{min} , that have to be used in order to achieve a desired accuracy.

4.3 BTD construction by means of genetic algorithms

The number of all possible combinations of active/not-active terms for a given refined model is equal to 2^M , where M is the number of terms (i.e. degrees of freedom) of the model. In the case of an ESL model, M can be computed as $M = (N + 1)3$. In the case of a LW model, $M = 3(N - 1)N_L$ since, as mentioned above, some terms of the displacement field cannot be discarded to impose the interface compatibility. As the expansion order increases, the number of the combinations to consider increases. The computational cost required for the BTD construction can be very significant. In order to construct BTDs with a lower computation effort, a different strategy was employed that was based on genetic algorithms.

The genetic algorithms are inspired by the evolution theory explained in "The origin of species", written by Darwin ([36]). In nature, weak and unfit individuals within their environment are faced with extinction by natural selection. The strong ones have a greater opportunity to pass their genes down to future generations via reproduction. In the long run, the species carrying the correct combination in their genes become dominant in their population. Sometimes, during the slow process of evolution, random changes may occur in the genes. If these changes provide additional advantages within the challenge of survival, new species evolve from the old ones. Unsuccessful changes are eliminated by natural selection. In the genetic algorithm terminology, a solution vector $\mathbf{x} \in \mathbf{X}$, where \mathbf{X} is the solution space, is called *individual* or *chromosome*. Individuals are made of discrete units called *genes*. Each gene controls one or more features of the individual. The present genetic algorithm use the *mutation* operator to generate new solutions from existing ones. The mutation operator introduce random changes into the characteristics of the chromosome. Mutation is generally applied at the gene level. Each individual has a fitness value based on its rank in the population. The population is ranked according to

the dominance rule reported in [32]. The fitness of each chromosome is evaluated through the following formula:

$$r_i(\mathbf{x}_i, t) = 1 + nq(\mathbf{x}_i, t) \quad (28)$$

where $nq(\mathbf{x}, t)$ is the number of solutions that are dominated by \mathbf{x} at the generation t . A lower rank corresponds to a better solution.

In the present work, each plate theory has been considered as an individual. The genes are the terms of the expansion and each gene can be active or not active, the deactivation of a term is obtained by exploiting a penalty technique. A synthetic representation of this approach is shown in Fig. 4. The meaning of the symbols \blacktriangle and \triangle is reported in Table 2. Each individual is therefore described by the number of active terms and its error that is computed with respect to a reference solution. the dominance rule is applied through these two parameters in order to evaluate the individual fitness. The generation of new refined theories starting from a generic population is inspired to the reproduction of bacteria; for each individual (plate theory) a number of copies are created according to its dominance and then, a number of mutations are applied in order to vary the set of new individuals. The purpose of this analysis is to find the individuals which belong to the Pareto front, that is, the subset of individuals which are dominated by no other individuals. Via preliminary analyses, the number of generations, i.e. iterations, was set equal to 10 and the number of the initial population was set to 400. The error of the reduced models with respect to a reference solution was evaluated through the following formula:

$$e = 100 \frac{\sum_{i=1}^{N_p} |Q^i - Q_{\text{ref}}^i|}{\max Q_{\text{ref}}} \cdot \frac{1}{N_p} \quad (29)$$

where Q can be a stress/displacement component (σ_{xx} in this paper) and N_p is the number of points along the thickness on which the entity Q is computed.

5 Results and discussion

The results of the axiomatic/asymptotic analyses are reported hereafter. A transverse pressure was applied to the top surface of the plate,

$$p_z = p_z^0 \sin\left(\frac{m\pi}{a}x\right) \sin\left(\frac{n\pi}{b}y\right) \quad (30)$$

where $m = n = 1$. The reference system layout is reported in Fig. 1. All the reduced models are developed for stress σ_{xx} , which is computed at $[a/2, b/2, z]$ with $-\frac{h}{2} \leq z \leq \frac{h}{2}$, where h is the total thickness of the plate.

5.1 Metallic plate

A metallic plate was first considered. The material properties are $E = 73$ GPa and $\nu = 0.34$ (aluminum). The length-to-thickness ratios (a/h) are equal to 2.5, 5 and 50.

First, an ED4 model assessment was carried out. The results are reported in Table 3; the three-dimensional exact elasticity results are obtained as in [37, 38]. It is possible to note that the results offered by the ED4 model are in excellent agreement with the reference solution. This makes the ED4 model suitable for the computation of the reference solution of the axiomatic/asymptotic analysis for the metallic plate. Table 4 reports the top and bottom values of σ_{xx} .

The first method that was used to build the BTD is based on the evaluation of all the possible combinations given by the 15 terms of an ED4 model, that is, $2^{15} = 32768$ theories; Fig. 5a shows the error of each theory. It is possible to note that some empty regions are present, and these regions are labeled as 1 and 2 in the figure. In this case, it is possible to state that the construction of reduced refined models is not always possible; in fact, there are no reduced models within some error intervals. The BTD is given by those combinations (i.e. plate theories) which, for a given error, require the lowest number of unknown variables. Two

BTDs are shown in Fig. 5, where the "All Combinations" BTD was built by evaluating all the 2^{15} combinations. The "Genetic" curve was built by exploiting a genetic algorithm. The genetic algorithm for the axiomatic/asymptotic technique evaluates around 400 individuals for 10 generations, this means that only about 4000 out of 32768 theories were evaluated. It is possible to note that almost all the models on the Pareto front were detected. The thickness locking was corrected in all those theories that have only linear or constant terms in the u_z displacement field. This choice is valid throughout this paper.

The influence of the plate geometry on BTD construction was considered, and the results are reported in Fig. 6. The curves suggest that, as a metallic plate becomes thinner, the BTD tends to be defined in a smaller region of the error/number-of-degrees-of-freedom plane (Error/NDOFs plane). Four classical theories from literature are also reported in the same graphs, that is, the CLT and FSDT theories and the theories of Pandya ([34]) and Kant ([35]). As the plate becomes thinner (i.e. a/h increases), the accuracy of the classical models increases. It is worth noting that none of the four models lie on the BTD. This means that for this problem and by considering σ_{xx} either the accuracy of the classical models can be achieved with fewer unknown variables, or that it is possible to obtain a better accuracy with the same number of variables. It can be noted that, for the thin plate case ($a/h = 50$), the best accuracy is given by a 13-term theory, that is, two terms in an ED4 model are not effective for the particular problem considered. In addition, the accuracy offered by 10, 11 and 12 term models is almost equal to the accuracy offered by the 13-term theory.

It is possible to detect different plate theories that compute the required output with a different approximation by keeping the number of active terms constant. These models are labeled 1, 2, and 3 (Fig. 6). Models 1, 2 and 3 and their errors are reported in Table 5 in which M_E indicates the ratio between the number of active variables and the number of the full model variables. It is possible to note that, for moderately thick and thin plates, the models that offer the lowest possible error have the same term arrangement. In addition, the models that belong to the BTD (models 1) have the terms u_{x1} , u_{z1} , u_{x2} , u_{y2} and u_{z2} in common. It is worth noting that, for a given plate geometry, the relevance of a term cannot be predicted easily. As an example, by considering the models labeled 1, 2 and 3 for $a/h = 2.5$, the term u_{y4} is included in models 2 and 3, but is not included in model 1. Examples of the explicit form of the reduced refined models are reported hereafter,

$$\begin{array}{lcl}
\text{Model 1, } a/h=2.5 & \begin{array}{l} u_x = u_{x1} + z u_{x2} + \quad \quad + z^3 u_{x4} \\ u_y = \quad \quad z u_{y2} \\ u_z = z1 + z u_{z2} + \quad \quad + z^3 u_{z4} \end{array} & \\
\hline
\text{Model 2, } a/h=5 & \begin{array}{l} u_x = u_{x1} + z u_{x2} + \quad \quad + z^3 u_{x4} \\ u_y = \quad \quad z u_{y2} \\ u_z = u_{z1} + z u_{z2} + z^2 u_{z3} \end{array} & (31) \\
\hline
\text{Model 3, } a/h=50 & \begin{array}{l} u_x = u_{x1} + z u_{x2} \\ u_y = \quad \quad z u_{y2} \\ u_z = u_{z1} + z u_{z2} + z^2 u_{z3} + z^3 u_{z4} + z^3 u_{x4} \end{array} &
\end{array}$$

The σ_{xx} distributions along the thickness are reported for different plate thickness in Fig. 7. The evaluation of the σ_{xx} stress is performed by means of the reduced models reported in Table 5. It can be noted that the stress distributions computed by means of the reduced models, which belong to the BTD (i.e. the models labeled as 1), are in perfect agreement with the reference solution. Moreover, it is possible to state that, for a given error interval, as a plate becomes thinner, different reduced models are able to compute the stress distribution with high accuracy. The results herein reported for the metallic plate suggest that

- for a given problem, it is possible to define a BTD that represents the set of reduced models which offer the lowest possible error with respect to a reference solution;
- a genetic algorithm makes it possible to construct a BTD with a lower computational cost;

- it is difficult to predict the relevant terms for a given problem;
- in most cases, the BTM models allow one to obtain better accuracies than classical models with the same number of variables, or to have the same accuracy with fewer variables.

5.2 Laminated plates

Axiomatic/asymptotic analysis results are reported for ED4 and LD4 models, considering symmetric and asymmetric laminated plates. The reference results have been obtained by means of the LD4 model. The assessment reported in Table 6 proves that LD4 model offers results that are in excellent agreement with the exact solutions available in the open literature. The exact solutions are taken from [39] and [40], and the material properties are $E_L/E_T = 25$, $G_{LT}/E_T = 0.5$, $G_{TT}/E_T = 0.2$, $\nu_{LT} = \nu_{TT} = 0.25$. In the following, the axiomatic/asymptotic analyses consider laminated plates whose layer properties are $E_L = 40 \times 10^9$ Pa, $E_T = E_z = 1 \times 10^9$ Pa, $G_{LT} = 0.5 \times 10^9$ Pa, $G_z = 0.6 \times 10^9$ Pa, $\nu = 0.25$. The ply sequences considered are $0^\circ/90^\circ/0^\circ$ for the symmetric plate and $0^\circ/90^\circ$ for the asymmetric plate; each layer has the same thickness. For the sake of brevity, only the most significant values of the stress distribution employed as a reference solution are reported in Tables 7 (symmetric case) and 8 (asymmetric case). The ED4 model BTMs for different plate geometries are reported in Figs 8 and 9, for a symmetric and an asymmetric plate, respectively. Comparing the BTMs for the two type of plates, it is possible to observe that the BTMs for the symmetric plates are defined in a smaller error interval than the BTMs for the asymmetric plate. It is worth noting that the maximum number of terms considered for all the BTMs reported is not equal to the total number of all the displacement variables of the ED4 model (15). It is possible to state that, in some cases, some terms of an ED4 model are ineffective. CLT, FSDT, Pandya and Kant model accuracies are also reported. It can be stated that, as a plate becomes thinner, the accuracy of the models increases, although none of them belongs to the BTMs. This means, as already mentioned for the metallic plate case, that either the accuracy of these models can be improved by considering a different term disposition (constant number of terms), or that their computational cost can be reduced considering a smaller number of terms (constant accuracy). Three additional models are also reported in Figs 8 and 9, and are labeled 1, 2 and 3. These models have the same number of terms, and they show that, for a given number of terms, it is possible to detect different theories that provide different accuracies. The equivalent model representations are reported in Tables 9 and 10, for symmetric and asymmetric plates, respectively. The reduced models for the symmetric plate reported in Table 9 underline that models which belong to the BTM are similar in some cases; the models labeled 1 for the thick and moderately thick plates ($a/h = 2.5 \div 5$) are identical. It is possible to conclude that, for a symmetric plate, the reduced models that were found for a particular problem can be profitably used in some cases to analyze different geometrical configurations. In the case of an asymmetric plate (Table 10), it can be noted that the reduced models which belong to the BTM curves mainly present the displacement variables related to the u_x expansion, this is due to the fact that σ_{xx} is being considered. As already noted for the ED4 model related to a metallic plate, the relevance of the terms for a given geometry cannot be predicted easily. The positions of all the ED4 reduced models in the Error/NDOFs plane are reported in Fig. 10, considering a thick asymmetric plate. The number of evaluated combinations is equal to 32768 (2^{15}). In this case, and in the following ones, the reported BTMs are obtained only by means of the genetic algorithm: around 400 individuals are considered for 10 generations. It can be noted that all the models which belong to the BTM are detected, although a fraction of all the possible combinations is considered ($400 \times 10/32768 = 4000/32768$). It should be underlined that the 15-term and 14-term models are not included in the BTM since they offer same accuracy as the 13-term model, but with a higher computational cost. Moreover, it is worth noting that no empty region is present, unlike the case reported in Fig. 5a. The stress distribution for the symmetric and asymmetric plates are reported in Figs 11 and 12, respectively. It can be noted that the reduced models which belong to the BTM make it possible to compute distributions that are in agreement with the reference solution. In addition, it can be noted that as the a/h increases, more reduced models are able to provide a satisfactory stress distribution.

BTDs are considered for LD4 models hereafter. The results are reported for the symmetric case in Fig. 13, and for the asymmetric case in Fig. 14. It can be observed that, as already noted for the ED4 models, as a plate becomes thinner, the error interval in which the BTD curves are defined reduces. In order to highlight the effect of the error and of the number of terms on the selection of the terms, the models labeled 1T, 2T, 3T, 1E, 2E and 3E are reported. Models 1T, 2T and 3T are obtained for a constant number of terms, and their synthetic representation is reported in Tables 11 and 12 for symmetric and asymmetric plates, respectively. Considering the reduced models for both types of plate, it is possible to observe that, as a plate becomes thinner, fewer higher-order terms are necessary. This is particularly evident for the symmetric plate (Table 11): the fourth-order terms are only present in the reduced models for the thick plate ($a/h = 2.5, 5$). It can again be noted that the relevance of the terms cannot be easily predicted. The models labeled 1E, 1E and 3E are obtained for a constant error. The relative synthetic representations are reported in Tables 13 (symmetric plate) and 14 (asymmetric plate). It should be mentioned that, like the constant number-of-term case, it is not easy to predict which terms are included, as a different total number of terms is considered. The positions of all the LD4 reduced models in the Error/NDOFs plane are reported in Fig. 15, considering a thick asymmetric plate. The number of evaluated combinations is equal to 262144 (2^{18}). Around 400 individuals are considered for 10 generations. It can be noted that all the models which belong to the BTD are detected, although a fraction of all the possible combinations is considered ($400 \times 10/262144 = 4000/262144$). The presence of empty regions can be observed for the LD4 model, these regions are labeled 1 and 2. The stress distributions are reported in Fig. 16 and 17 (symmetric and asymmetric plates, respectively), where it is possible to observe the good agreement with the reference solution and, as already noted for the ED4 model, it is possible to state that, for a given error interval, as a plate becomes thinner, different models can be used successfully. The analyses reported for the laminated plates suggest that

- a BTD can be built by considering ESL and LW approaches; in addition.
- Genetic algorithms are very effective in building BTDs since far fewer model combinations are needed.
- It is difficult to predict which terms can be included in a reduced model.
- The computational cost reduction given by the reduced models is generally far more evident in the LW models than in the ESL models.

6 Conclusion

The axiomatic/asymptotic technique has been employed to detect the "best" reduced models for ESL and LW that belong to Best Theory Diagrams (BTDs). The BTDs have been reported for different problems, considering different geometries (length-to-thickness ratio, a/h) and material properties. Simply-supported plates have been analyzed by means of the CUF and an analytical solution (Navier-type) has been employed. A genetic-like algorithm has been employed in order to build BTDs. The following conclusions may be drawn:

1. for a given model, plate geometry and material configuration, it is possible to identify a number of reduced models which present the lowest possible error; in other words, it is possible to define a Best Theory Diagram (BTD).
2. the axiomatic/asymptotic technique, conducted by means of the genetic algorithm, is able to detect the reduced models that belong to the BTD;
3. in the case of the ED4 and LD4 models, it has been found that, for a given model, problem and interval in the Error/NDOFs plane, it is not always possible to define a reduced model;
4. the geometric parameter (a/h) and the material properties influence the selection of terms;

5. the classical and refined models reported in the literature are accurate, although, according to the results here reported for a given problem and output (σ_{xx} in this paper), either higher accuracies can be achieved (constant number of terms) or lower computational costs can be obtained (constant accuracy);
6. the relevance of the terms for a model cannot be predicted easily as the error (constant term number) or the total amount of active terms (constant accuracy) vary.

The CUF theory has proved to be a useful means of generating refined models and of considering the accuracy of the results as an input. In addition, the use of the analytical solution has made it possible to compute the error of a large number of combinations of terms with a low computational effort. In the future, the present approach could be applied to multifield problems and shell/beam models.

Appendix: fundamental nucleus components

The nine components of the fundamental nucleus for a generic layer k are herein reported explicitly

$$\begin{aligned}
\hat{K}_{11}^{k\tau s} &= -\tilde{C}_{11}^k E_{\tau s} \partial_{,x}^2 - \tilde{C}_{16}^k E_{\tau s} \partial_{,xy}^2 - \tilde{C}_{16}^k E_{\tau s} \partial_{,yx}^2 - \tilde{C}_{66}^k E_{\tau s} \partial_{,y}^2 + \tilde{C}_{55}^k E_{\tau,z s,z} \\
\hat{K}_{12}^{k\tau s} &= -\tilde{C}_{12}^k E_{\tau s} \partial_{,xy}^2 + \tilde{C}_{16}^k E_{\tau s} \partial_{,x}^2 - \tilde{C}_{26}^k E_{\tau s} \partial_{,y}^2 - \tilde{C}_{66}^k E_{\tau s} \partial_{,yx}^2 + \tilde{C}_{45}^k E_{\tau,z s,z} \\
\hat{K}_{13}^{k\tau s} &= -\tilde{C}_{13}^k E_{\tau,z s} \partial_{,x} - \tilde{C}_{36}^k E_{\tau,z s} \partial_{,y} + \tilde{C}_{55}^k \partial_{,x} E_{\tau s,z} + \tilde{C}_{45}^k \partial_{,y} E_{\tau s,z} \\
\hat{K}_{21}^{k\tau s} &= -\tilde{C}_{12}^k E_{\tau s} \partial_{,yx}^2 - \tilde{C}_{26}^k E_{\tau s} \partial_{,y}^2 - \tilde{C}_{16}^k E_{\tau s} \partial_{,x}^2 - \tilde{C}_{66}^k E_{\tau s} \partial_{,xy}^2 + \tilde{C}_{45}^k E_{\tau,z s,z} \\
\hat{K}_{22}^{k\tau s} &= -\tilde{C}_{22}^k E_{\tau s} \partial_{,y}^2 - \tilde{C}_{26}^k E_{\tau s} \partial_{,yx}^2 - \tilde{C}_{26}^k E_{\tau s} \partial_{,xy}^2 + \tilde{C}_{66}^k E_{\tau s} \partial_{,x}^2 + \tilde{C}_{44}^k E_{\tau,z s,z} \\
\hat{K}_{23}^{k\tau s} &= -\tilde{C}_{23}^k E_{\tau,z s} \partial_{,y} - \tilde{C}_{36}^k E_{\tau,z s} \partial_{,x} + \tilde{C}_{45}^k \partial_{,x} E_{\tau s,z} + \tilde{C}_{44}^k \partial_{,y} E_{\tau s,z} \\
\hat{K}_{31}^{k\tau s} &= -\tilde{C}_{55}^k E_{\tau,z s} \partial_{,x} - \tilde{C}_{45}^k E_{\tau,z s} \partial_{,y} + \tilde{C}_{13}^k \partial_{,x} E_{\tau s,z} + \tilde{C}_{36}^k \partial_{,y} E_{\tau s,z} \\
\hat{K}_{32}^{k\tau s} &= -\tilde{C}_{45}^k E_{\tau,z s} \partial_{,x} - \tilde{C}_{44}^k E_{\tau,z s} \partial_{,y} + \tilde{C}_{23}^k \partial_{,y} E_{\tau s,z} + \tilde{C}_{36}^k \partial_{,x} E_{\tau s,z} \\
\hat{K}_{33}^{k\tau s} &= -\tilde{C}_{55}^k E_{\tau s} \partial_{,x}^2 - \tilde{C}_{45}^k E_{\tau s} \partial_{,xy}^2 - \tilde{C}_{54}^k E_{\tau s} \partial_{,yx}^2 - \tilde{C}_{44}^k E_{\tau s} \partial_{,y}^2 + \tilde{C}_{33}^k E_{\tau,z s,z} \quad (32)
\end{aligned}$$

Symbols $\partial_{,xx}^2$, $\partial_{,yy}^2$, $\partial_{,xy}^2$, $\partial_{,x}$ and $\partial_{,y}$ denote synthetically the differential operators $\frac{\partial^2}{\partial x^2}$, $\frac{\partial^2}{\partial y^2}$, $\frac{\partial^2}{\partial x \partial y}$, $\frac{\partial}{\partial x}$ and $\frac{\partial}{\partial y}$. The components of the fundamental nucleus for the boundary conditions considering a generic layer k are

$$\begin{aligned}
\hat{\Pi}_{11}^{k\tau s} &= \tilde{C}_{11}^k E_{\tau s} \partial_{,x} + \tilde{C}_{16}^k E_{\tau s} \partial_{,y} + \tilde{C}_{16}^k E_{\tau s} \partial_{,x} + \tilde{C}_{66}^k E_{\tau s} \partial_{,y} \\
\hat{\Pi}_{12}^{k\tau s} &= \tilde{C}_{12}^k E_{\tau s} \partial_{,y} + \tilde{C}_{16}^k E_{\tau s} \partial_{,x} + \tilde{C}_{26}^k E_{\tau s} \partial_{,y} + \tilde{C}_{66}^k E_{\tau s} \partial_{,x} \\
\hat{\Pi}_{13}^{k\tau s} &= \tilde{C}_{13}^k E_{\tau,z s} - \tilde{C}_{36}^k E_{\tau,z s} \\
\hat{\Pi}_{21}^{k\tau s} &= \tilde{C}_{12}^k E_{\tau s} \partial_{,x} + \tilde{C}_{26}^k E_{\tau s} \partial_{,y} + \tilde{C}_{16}^k E_{\tau s} \partial_{,x} + \tilde{C}_{66}^k E_{\tau s} \partial_{,y} \\
\hat{\Pi}_{22}^{k\tau s} &= \tilde{C}_{22}^k E_{\tau s} \partial_{,y} + \tilde{C}_{26}^k E_{\tau s} \partial_{,x} + \tilde{C}_{26}^k E_{\tau s} \partial_{,xy} + \tilde{C}_{66}^k E_{\tau s} \partial_{,x} \\
\hat{\Pi}_{23}^{k\tau s} &= \tilde{C}_{13}^k E_{\tau,z s} - \tilde{C}_{36}^k E_{\tau,z s} \\
\hat{\Pi}_{31}^{k\tau s} &= \tilde{C}_{55}^k E_{\tau,z s} + \tilde{C}_{45}^k E_{\tau,z s} \\
\hat{\Pi}_{32}^{k\tau s} &= \tilde{C}_{45}^k E_{\tau,z s} + \tilde{C}_{44}^k E_{\tau,z s} \\
\hat{\Pi}_{33}^{k\tau s} &= \tilde{C}_{55}^k E_{\tau s} \partial_{,x} - \tilde{C}_{45}^k E_{\tau s} \partial_{,y} - \tilde{C}_{54}^k E_{\tau s} \partial_{,x} - \tilde{C}_{44}^k E_{\tau s} \partial_{,y} \quad (33)
\end{aligned}$$

References

- [1] G. Kirchhoff. Uber das gleichgewicht und die bewegung einer elastischen scheibe. *Journal fur reins und angewandte Mathematik*, 40:51–88, 1850. doi: 10.1515/crll.1850.40.51.
- [2] A. E. H. Love. *The Mathematical Theory of Elasticity*. Cambridge University Press, Cambridge, 1927.
- [3] E. Reissner. The effect of transverse shear deformation on the bending of elastic plates. *Journal of Applied Mechanics*, 12:69–76, 1945. doi: 10.1515/crll.1850.40.51.
- [4] R. D. Mindlin. Influence of rotatory inertia and shear in flexural motions of isotropic elastic plates. *Journal of Applied Mechanics*, 18:1031–1036, 1951. doi: 10.1515/crll.1850.40.51.
- [5] B. F. Vlasov. On the equations of bending of plates. *Doklady Akademii Nauk Azerbaidzhan-skoi SSR*, 3:955–979, 1957. doi: 10.1515/crll.1850.40.51.
- [6] F.B. Hildebrand, E. Reissner, and Thomas G.B. Notes in the foundations of the theory of small displacement of orthotropic shells. Technical Report NACA TN-1833, NASA, March 1949.
- [7] E. Carrera. A class of two dimensional theories for multilayered plates analisys. *Atti Acc. Sci. Torino*, 19-20:49–87, 1995.
- [8] E. Carrera. c_z^0 requirements - models for the two dimensional analysis of multilayered structures. *Composite Structures*, 37(3-4):373–383, 1997. [http://dx.doi.org/10.1016/S0263-8223\(98\)80005-6](http://dx.doi.org/10.1016/S0263-8223(98)80005-6).
- [9] E. Carrera. Historical review of zig-zag theories for multilayered plates and shells. *Applied Mechanics Reviews*, 56(3):287–308, 2003.
- [10] G. S. Lekhnitskii. *Anisotropic Plates*, 2nd edition. SW Tsai and Cheron, Bordon and Breach, 1968.
- [11] S. A. Ambartsumian. Contributions to the theory of anisotropic layered shells. *Applied Mechanics Reviews*, 15(4):245–249, 1962. doi: 10.1515/crll.1850.40.51.
- [12] E. Reissner. On a certain mixed variational theory and a proposed application. *International Journal for Numerical Methods in Engineering*, 20:1366–1368, 1984.
- [13] E. Reissner. Reflections on the theory of elastic plates. *Applied Mechanics Review*, 38:1453–1464, 1985.
- [14] E. Reissner. On a mixed variational theorem and on a shear deformable plate theory. *International Journal for Numerical Methods in Engineering*, 23:193–198, 1986.
- [15] E. Reissner. On a certain mixed variational theorem and on laminated elastic shell theory. *Proceedings of the Euromech-Colloquium*, 219:17.27, 1986.
- [16] J. N. Reddy. *Mechanics of Laminated Plates, Theory and Analysis*. CRC Press, Boca Raton, 1997.
- [17] E. Carrera, S. Brischetto, and P. Nali. *Plates and Shells for Smart Structures Classical and Advanced Theories for Modeling and Analysis*. John Wiley & Sons, Inc., 2011.
- [18] E. Carrera, G. Giunta, and M. Petrolo. *Beam Structures, Classical and Advanced Theories*. John Wiley & Sons, Inc., 2011.
- [19] E. Carrera, M. Cinefra, M. Petrolo, and E. Zappino. *Finite Element Analysis of Structures through Unified Formulation*. John Wiley & Sons, Inc., 2014.

- [20] E. Carrera. Theories and finite elements for multilayered plates and shells: A unified compact formulation with numerical assessment and benchmarking. *Arch. Comput. Meth. Engng*, 10(3):215–296, 2003.
- [21] E. Carrera and M. Petrolo. Guidelines and recommendation to construct theories for metallic and composite plates. *AIAA Journal*, 48(12):2852–2866, 2010. doi: 10.2514/1.J050316.
- [22] E. Carrera, F. Miglioretti, and M. Petrolo. Accuracy of refined finite elements for laminated plate analysis. *Composite Structures*, 93:1311 – 1327, 2010. doi: 10.1016/j.compstruct.2010.11.007.
- [23] E. Carrera and M. Petrolo. On the effectiveness of higher-order terms in refined beam theories. *Journal of Applied Mechanics*, 78:1 – 17, 2011. doi: 10.1115/1.4002207.
- [24] E. Carrera, F. Miglioretti, and M. Petrolo. Computations and evaluations of higher order theories for free vibration analysis of beams. *Journal of Sound and Vibration*, 331:4269–4284, 2012. doi:http://dx.doi.org/10.1016/j.jsv.2012.04.017.
- [25] M. Petrolo and A. Lamberti. Axiomatic/asymptotic analysis of refined layer-wise theories for composite and sandwich plates. *Mechanics of Advanced Materials and Structures*, 2014. In press, doi: 10.1080/15376494.2014.924607.
- [26] D. S. Mashat, E. Carrera, A. M. Zenkour, and S. A. Al Khateeb. Use of axiomatic/asymptotic approach to evaluate various refined theories for sandwich shells. *Composite Structures*, 109(0):139–149, 2013. doi: http://dx.doi.org/10.1016/j.compstruct.2013.10.046.
- [27] D. S. Mashat, E. Carrera, A. M. Zenkour, and S. A. Al Khateeb. Axiomatic/asymptotic evaluation of multilayered plate theories by using single and multi-points error criteria. *Composite Structures*, 106(0):393–406, 2013. doi: http://dx.doi.org/10.1016/j.compstruct.2013.05.047.
- [28] E. Carrera, F. Miglioretti, and M. Petrolo. Guidelines and recommendations on the use of higher order finite elements for bending analysis of plates. *International Journal for Computational Methods in Engineering Science and Mechanics*, 12(6):303–324, 2011. doi:10.1080/15502287.2011.615792.
- [29] E. Carrera and F. Miglioretti. Selection of appropriate multilayered plate theories by using a genetic like algorithm. *Composite Structures*, 94(3):1175 – 1186, 2012. doi: http://dx.doi.org/10.1016/j.compstruct.2011.10.013.
- [30] J. Holland. *Adaptation in natural and artificial system*. University Michigan Press, 1975.
- [31] K. Abdullah, W. David, and E. Alice. Multi-objective optimization using genetic algorithms: a tutorial. *Reliab Eng Syst Safety*, 91:992 – 1007, 2006.
- [32] M. Fonseca and P. Fleming. Genetic algorithm for multiobjective optimization: formulation, discussion and generalization. In *Genetic algorithms: proceedings of the fifth international conference*, pages 416 – 423, 1993.
- [33] Gbor R. and E. Anik. Genetic algorithms in computer aided design. *Comput-Aid Des*, 35:709 – 726, 2003.
- [34] B. Pandya and T. Kant. Finite element analysis of laminated compiste plates using high-order displacement model. *Compos Sci Technol*, 32:137–55, 1988.
- [35] T. Kant and B. Manjunatha. An unsymmetric FRC laminate C^0 finite element model with 12 degrees of freedom per node. *Eng Comput*, 5(3):292–308, 1988.
- [36] C. R. Darwin. *On the origin of species by means of natural selection, or the preservation of favored races in the struggle for life*. John Murray, London, 1859.

- [37] E. Carrera, G. Giunta, and S. Brischetto. Hierarchical closed form solutions for plates bent by localized transverse loadings. *Journal of Zhejiang University Science B*, 8(7):1026–1037, 2007. doi:10.1631/jzus.2007.A1026.
- [38] E. Carrera and G. Giunta. Hierarchical models for failure analysis of plates bent by distributed and localized transverse loadings. *Journal of Zhejiang University Science A*, 9(5):6020–613, 2008. doi:10.1631/jzus.A072110.
- [39] N. J. Pagano. Exact solutions for rectangular bidirectional composites and sandwich plate. *Journal of Composites Material*, 4:20–34, 1969.
- [40] N. J. Pagano. Elastic behavior of multilayered bidirectional composites. *AIAA Journal*, 10(7):931–933, 1972.

Figure Caption List

1. Figure 1: Plate geometry and notation.
2. Figure 2: Linear and higher-order ESL and LW examples.
 - Figure 2a: Equivalent Single Layer scheme.
 - Figure 2b: Layer Wise scheme.
3. Figure 3: NDOFs vs error plot example.
4. Figure 4: Displacement variables of a refined model and genes of an individual.
5. Figure 5: Genetic algorithm assessment, ED4 reduced models, metallic plate, $a/h = 2.5$.
 - Figure 5a: BTD.
 - Figure 5b: BTD for error $< 7\%$.
6. Figure 6: BTDs for simply-supported metallic plates, ED4 reduced models for different a/h .
 - Figure 6a: $a/h = 50$.
 - Figure 6b: $a/h = 5$.
 - Figure 6c: $a/h = 2.5$.
7. Figure 7: σ_{xx} distribution along the thickness for metallic plates, ED4 reduced models, reduced models from Table 5.
 - Figure 7a: $a/h = 50$.
 - Figure 7b: $a/h = 5$.
 - Figure 7c: $a/h = 2.5$.
8. Figure 8: BTDs for simply-supported symmetric laminated plates, ED4 reduced models for different a/h .
 - Figure 8a: $a/h = 50$.
 - Figure 8b: $a/h = 5$.
 - Figure 8c: $a/h = 2.5$.
9. Figure 9: BTDs for simply-supported asymmetric laminated plates, ED4 reduced models for different a/h .
 - Figure 9a: $a/h = 50$.
 - Figure 9b: $a/h = 5$.
 - Figure 9c: $a/h = 2.5$.
10. Figure 10: Genetic algorithm assessment, ED4 reduced models, asymmetric laminated plate, $a/h = 2.5$.
11. Figure 11: σ_{xx} distribution along the thickness for symmetric laminated plates, ED4 reduced models, reduced models from Table 9.
 - Figure 11a: $a/h = 50$.
 - Figure 11b: $a/h = 5$.
 - Figure 11c: $a/h = 2.5$.

12. Figure 12: σ_{xx} distribution along the thickness for asymmetric laminated plates, ED4 reduced models, reduced models from Table 10.
 - Figure 12a: $a/h = 50$.
 - Figure 12b: $a/h = 5$.
 - Figure 12c: $a/h = 2.5$.
13. Figure 13: BTDs for simply-supported symmetric laminated plates, LD4 reduced models for different a/h .
 - Figure 13a: $a/h = 50$.
 - Figure 13b: $a/h = 5$.
 - Figure 13c: $a/h = 2.5$.
14. Figure 14: BTDs for simply-supported asymmetric laminated plates, LD4 reduced models for different a/h .
 - Figure 14a: $a/h = 50$.
 - Figure 14b: $a/h = 5$.
 - Figure 14c: $a/h = 2.5$.
15. Figure 15: Genetic algorithm assessment, LD4 reduced models, asymmetric laminated plate, $a/h = 2.5$.
16. Figure 16: σ_{xx} distribution along the thickness for symmetric laminated plates, LD4 reduced models, reduced models from Table 11.
 - Figure 16a: $a/h = 50$.
 - Figure 16b: $a/h = 5$.
 - Figure 16c: $a/h = 2.5$.
17. Figure 17: σ_{xx} distribution along the thickness for asymmetric laminated plates, LD4 reduced models, reduced models from Table 12.
 - Figure 17a: $a/h = 50$.
 - Figure 17b: $a/h = 5$.
 - Figure 17c: $a/h = 2.5$.

Table Caption List

1. Table 1: Model representations.
2. Table 2: Symbols to indicate the status of a displacement variable.
3. Table 3: ED4 model assessment for the metallic plate, $\bar{\sigma}_{xx} = \frac{\sigma_{xx}}{p_z^0 (a/h)^2}$.
4. Table 4: ED4 model assessment for the metallic plate, top and bottom $\bar{\sigma}_{xx}$ values.
5. Table 5: ED4 reduced models for a simply-supported isotropic plate for different accuracies and constant number of terms.
6. Table 6: Stresses and displacement for 3-layer and a 5-layer simply-supported laminated plates, $\bar{u}_z = \frac{u_z 100 E_T h^3}{p_z^0 a^4}$, $\bar{\sigma}_{xx/yy/xy} = \frac{\sigma_{xx/yy/xy}}{p_z^0 (a/h)^2}$, $\bar{\sigma}_{xz/yz} = \frac{\sigma_{xz/yz}}{p_z^0 (a/h)}$.
7. Table 7: ED4 and LD4 model assessments for the symmetric plate, top and bottom $\bar{\sigma}_{xx}$ values.

8. Table 8: ED4 and LD4 model assessments for the asymmetric plate, top and bottom $\bar{\sigma}_{xx}$ values.
9. Table 9: ED4 reduced models for a simply-supported symmetric plate for different accuracies and constant number of terms.
10. Table 10: ED4 reduced models for a simply-supported asymmetric plate for different accuracies and constant number of terms.
11. Table 11: LD4 reduced models for a simply-supported symmetric plate for different accuracies and constant number of terms ($M_E = 18/39$).
12. Table 12: LD4 reduced models for a simply-supported asymmetric plate for different accuracies and constant number of terms ($M_E = 15/27$).
13. Table 13: LD4 reduced models for a simply-supported symmetric plate for given accuracies and different number of terms.
14. Table 14: LD4 reduced models for a simply-supported asymmetric plate for given accuracies and different number of terms.

Tables

Full model representation									Reduced model representation								
■	▲	▲	▲	■	▲	▲	▲	■	■	▲	▲	▲	■	△	▲	▲	■
■	▲	▲	▲	■	▲	▲	▲	■	■	▲	▲	▲	■				
■	▲	▲	▲	■	▲	▲	▲	■	■	△	▲	▲	■	▲	▲	▲	■

Table 1: Model representations

Table 2: Symbols to indicate the status of a displacement variable.

Active term	Inactive term	Non-deactivable term
\blacktriangle	\triangle	\blacksquare

Table 3: ED4 model assessment for the metallic plate, $\bar{\sigma}_{xx} = \frac{\sigma_{xx}}{p_z^0 (a/h)^2}$.

a/h	100	10	5	2
Ref. [37, 38]	0.2037	0.2068	0.2168	0.3145
ED4	0.2037	0.2068	0.2168	0.3165

Table 4: ED4 model assessment for the metallic plate, top and bottom $\bar{\sigma}_{xx}$ values.

$a/h = 50$	$a/h = 5$	$a/h = 2.5$
ED4		
0.2038	0.2168	0.2680
-0.2037	-0.2083	-0.2145

Table 5: ED4 reduced models for a simply-supported isotropic plate for different accuracies and constant number of terms.

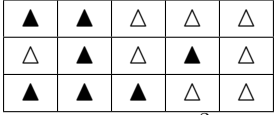
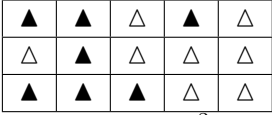
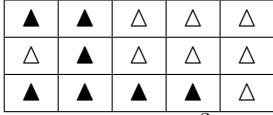
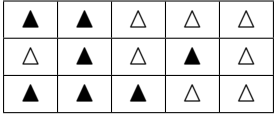
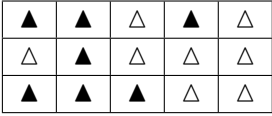
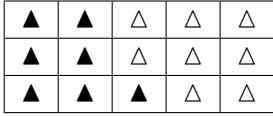
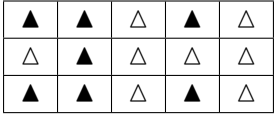
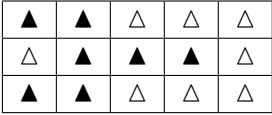
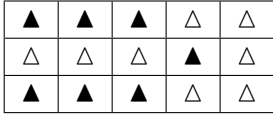
	1	2	3	M_E
		$a/h = 50$		
	<div>  </div>	<div>  </div>	<div>  </div>	7/15
Error	$5.0143 \times 10^{-3} \%$	$6.4419 \times 10^{-3} \%$	$9.8327 \times 10^{-3} \%$	
		$a/h = 5$		
	<div>  </div>	<div>  </div>	<div>  </div>	7/15
Error	0.5212 %	0.6510 %	0.9225 %	
		$a/h = 2.5$		
	<div>  </div>	<div>  </div>	<div>  </div>	7/15
Error	2.0478 %	2.8970 %	4.1000 %	

Table 6: Stresses and displacement for 3-layer and a 5-layer simply-supported laminated plates,
 $\bar{u}_z = \frac{u_z 100 E_T h^3}{p_z^0 a^4}$, $\bar{\sigma}_{xx/yy/xy} = \frac{\sigma_{xx/yy/xy}}{p_z^0 (a/h)^2}$, $\bar{\sigma}_{xz/yz} = \frac{\sigma_{xz/yz}}{p_z^0 (a/h)}$.

$a/h = 100$									
3-layer laminate									
	$\bar{\sigma}_{xx}(z = \pm h/2)$		$\bar{\sigma}_{yy}(z = \pm h/6)$		$\bar{\sigma}_{xz}(z = 0)$	$\bar{\sigma}_{yz}(z = 0)$	$\bar{\sigma}_{xy}(z = \pm h/2)$		
Ref. [39]	± 0.539		0.181		0.395	0.0828	∓ 0.0213		
LD4	± 0.539		0.181		0.395	0.0828	∓ 0.0214		
5-layer laminate									
	$\bar{\sigma}_{xx}(z = \pm h/2)$		$\bar{\sigma}_{yy}(z = \pm h/3)$		$\bar{\sigma}_{xz}(z = 0)$	$\bar{\sigma}_{yz}(z = 0)$	$\bar{u}_z(z = 0)$		
Ref. [40]	± 0.539		± 0.360		0.272	0.205	1.006		
LD4	± 0.539		± 0.360		0.272	0.206	1.006		
$a/h = 4$									
3-layer laminate									
	$\bar{\sigma}_{xx}(z = \pm h/2)$		$\bar{\sigma}_{yy}(z = \pm h/6)$		$\bar{\sigma}_{xz}(z = 0)$	$\bar{\sigma}_{yz}(z = 0)$	$\bar{\sigma}_{xy}(z = \pm h/2)$		
Ref. [39]	0.801	-0.755	0.534	-0.556	0.256	0.2172	-0.0511	0.0505	
LD4	0.801	-0.755	0.534	-0.556	0.256	0.2180	-0.0511	0.0505	
5-layer laminate									
	$\bar{\sigma}_{xx}(z = \pm h/2)$		$\bar{\sigma}_{yy}(z = \pm h/3)$		$\bar{\sigma}_{xz}(z = 0)$	$\bar{\sigma}_{yz}(z = 0)$	$\bar{u}_z(z = 0)$		
Ref. [40]	0.685	-0.651	0.633	-0.626	0.238	0.229	4.291		
LD4	0.685	-0.651	0.634	-0.626	0.238	0.229	4.291		

Table 7: ED4 and LD4 model assessments for the symmetric plate, top and bottom $\bar{\sigma}_{xx}$ values.

LD4		
$a/h = 50$	$a/h = 5$	$a/h = 2.5$
0.5636	0.6792	1.0802
-0.5637	-0.6500	-0.7573
ED4		
0.5635	0.6608	0.9736
-0.5635	-0.6314	-0.6646

Table 8: ED4 and LD4 model assessments for the asymmetric plate, top and bottom $\bar{\sigma}_{xx}$ values.

$a/h = 50$	$a/h = 5$	$a/h = 2.5$
LD4		
0.0642	0.0939	0.1665
-0.8374	-0.8532	-0.8473
ED4		
0.0641	0.0918	0.1636
-0.8371	-0.8357	-0.8077

Table 9: ED4 reduced models for a simply-supported symmetric plate for different accuracies and constant number of terms.

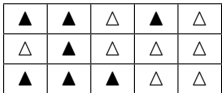
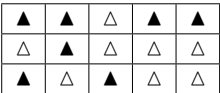

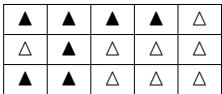

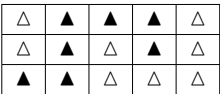
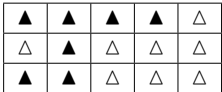
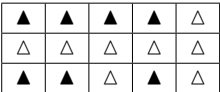

	1	2	3	M_E
		$a/h = 50$		
	<div>  </div>	<div>  </div>	<div>  </div>	7/15
Error	$2.0339 \times 10^{-2} \%$	$2.1568 \times 10^{-2} \%$	$2.2652 \times 10^{-2} \%$	
		$a/h = 5$		
	<div>  </div>	<div>  </div>	<div>  </div>	7/15
Error	1.7773 %	1.8510 %	2.0909 %	
		$a/h = 2.5$		
	<div>  </div>	<div>  </div>	<div>  </div>	7/15
Error	4.0948 %	6.2448 %	9.4185 %	

Table 10: ED4 reduced models for a simply-supported asymmetric plate for different accuracies and constant number of terms.

	1	2	3	M_E
		$a/h = 50$		
	<div> </div>	<div> </div>	<div> </div>	7/15
Error	$4.0673 \times 10^{-2} \%$	0.5226 %	31.1968 %	
		$a/h = 5$		
	<div> </div>	<div> </div>	<div> </div>	7/15
Error	2.8403 %	3.9886 %	5.6545 %	
		$a/h = 2.5$		
	<div> </div>	<div> </div>	<div> </div>	7/15
Error	10.9645 %	15.6582 %	24.9191 %	

Table 11: LD4 reduced models for a simply-supported symmetric plate for different accuracies and constant number of terms ($M_E = 18/39$).



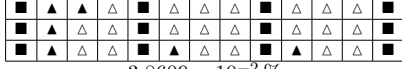






	1T	2T	3T
		$a/h = 50$	
Error	 $4.5882 \times 10^{-3} \%$	 $3.4133 \times 10^{-2} \%$	 $3.8609 \times 10^{-2} \%$
		$a/h = 5$	
Error	 0.1130%	 0.5008%	 2.5944%
		$a/h = 2.5$	
Error	 0.45682%	 1.6425%	 4.8606%

Table 12: LD4 reduced models for a simply-supported asymmetric plate for different accuracies and constant number of terms ($M_E = 15/27$).


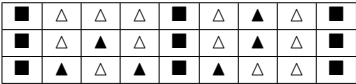
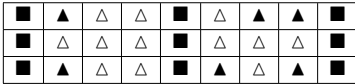
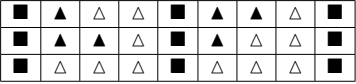

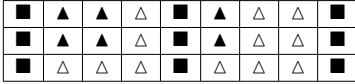
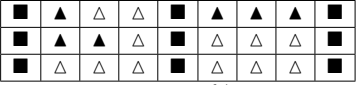

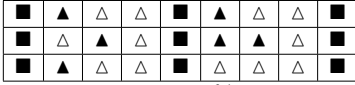
	1T	2T	3T
		$a/h = 50$	
Error	 $1.6834 \times 10^{-3} \%$	 $1.1191 \times 10^{-2} \%$	 $1.7970 \times 10^{-2} \%$
		$a/h = 5$	
Error	 0.1100%	 1.335%	 3.022%
		$a/h = 2.5$	
Error	 0.90182%	 4.1034%	 11.8300%

Table 13: LD4 reduced models for a simply-supported symmetric plate for given accuracies and different number of terms.

1E	2E	3E
	$a/h = 50$, Error = $6.3155 \times 10^{-2} \%$	
$M_E : 13/39$	$M_E : 14/39$	$M_E : 15/39$
	$a/h = 5$, Error = 2.2956%	
$M_E : 13/39$	$M_E : 14/39$	$M_E : 15/39$
	$a/h = 2.5$, Error = 2.2869%	
$M_E : 14/39$	$M_E : 15/39$	$M_E : 16/39$

Table 14: LD4 reduced models for a simply-supported asymmetric plate for given accuracies and different number of terms.

1E	2E	3E
$a/h = 50$, Error = $3.1659 \times 10^{-2} \%$		
$M_E : 11/27$	$M_E : 12/27$	$M_E : 13/27$
$a/h = 5$, Error = 0.9071 %		
$M_E : 11/27$	$M_E : 12/27$	$M_E : 13/27$
$a/h = 2.5$, Error = 4.4066 %		
$M_E : 11/27$	$M_E : 12/27$	$M_E : 13/27$